Topological interface states in the natural heterostructure $(PbSe)_5(Bi_2Se_3)_6$ with Bi_{Pb} defects

Hiroyoshi Momida,[1,2] Gustav Bihlmayer,[2] Stefan Blügel,[2] Kouji Segawa,[3] Yoichi Ando,[4] and Tamio Oguchi[1]
[1]*Institute of Scientific and Industrial Research, Osaka University, 8-1 Mihogaoka, Ibaraki, Osaka 567-0047, Japan*
[2]*Peter Grünberg Institut and Institute for Advanced Simulation, Forschungszentrum Jülich and JARA, 52425 Jülich, Germany*
[3]*Department of Physics, Kyoto Sangyo University, Kyoto 603-8555, Japan*
[4]*Physics Institute II, University of Cologne, Zülpicher Straße 77, 50937 Köln, Germany*

(Received 1 October 2017; published 9 January 2018)

We study theoretically the electronic band structure of $(PbSe)_5(Bi_2Se_3)_6$, which consists of an ordinary insulator PbSe and a topological insulator Bi_2Se_3. The first-principles calculations show that this material has a gapped Dirac-cone energy dispersion inside the bulk, which originates from the topological states of Bi_2Se_3 layers encapsulated by PbSe layers. Furthermore, we calculate the band structures of $(Bi_xPb_{1-x}Se)_5(Bi_2Se_3)_6$ with Bi_{Pb} antisite defects included in the PbSe layers. The result shows that a high density of Bi_{Pb} defects can exist in real materials, consistent with the experimentally estimated x of more than 30%. The Bi_{Pb} defects strongly modify the band alignment between Bi_2Se_3 and PbSe layers, while the topological interface states of Bi_2Se_3 are kept as a gapped Dirac-cone-like dispersion.

DOI: 10.1103/PhysRevB.97.035113

I. INTRODUCTION

The Pb-based homologous series of $(PbSe)_5(Bi_2Se_3)_{3m}$ ($m = 1,2$) have recently attracted attention and been studied experimentally because of their interesting and unconventional topological properties [1–6]. $(PbSe)_5(Bi_2Se_3)_{3m}$ consists of an alternating layered structure of m quintuple layers (QLs) of Bi_2Se_3 with bilayer PbSe [7,8], and it is naturally formed as a multilayer heterostructure. The bulk Bi_2Se_3 and PbSe materials are well known to be a topological and an ordinary insulator, respectively [1,9–12]. Therefore, we can expect that topological interface states exist at the Bi_2Se_3-PbSe boundaries inside the bulk. Such multilayer systems possessing a topological and an ordinary insulator have also been considered to be an interesting playground for realizing novel Weyl semimetal phases [13].

Nakayama *et al.* have observed gapped Dirac-cone dispersions within the bulk band gap for $m = 2$ via angle-resolved photoemission spectroscopy (ARPES), showing that topological interface states are effectively encapsulated by the PbSe block layers [2,3]. Prompted by recent interest in topological superconductors [14], an unconventional superconducting nature has been studied experimentally for $(PbSe)_5(Bi_2Se_3)_{3m}$-based materials with Ag doping [4] and Cu intercalations [3,5]. However, a detailed understanding of this material is very limited, especially from theoretical viewpoints. Thus, it is necessary to clarify the electronic band structure of $(PbSe)_5(Bi_2Se_3)_6$, especially near the Fermi energy region, using first-principles calculations.

Only a few reports on the detailed crystal structures of $(PbSe)_5(Bi_2Se_3)_{3m}$ are available. Fang *et al.* have shown the crystal structure information for $(PbSe)_5(Bi_2Se_3)_{3m}$ ($m = 1,2$) [4], and that $(PbSe)_5(Bi_2Se_3)_6$ belongs to the monoclinic space group $C2/m$, which includes inversion symmetry. Segawa *et al.* have successfully synthesized the $(PbSe)_5(Bi_2Se_3)_{3m}$ homologous series with $m = 1-4$, and they analyzed their atomic, structural, and transport properties [6]. They pointed out that the real materials intrinsically include high densities of Bi antisite defects at Pb sites (denoted as Bi_{Pb}), indicating that the actual chemical formula of their samples might be expressed as $(Bi_{0.31}Pb_{0.65}Se)_5(Bi_2Se_3)_6$ for the $m = 2$ material. The Bi_{Pb} antisites can be considered to be electron donors in the materials, but the actual influences of the defects on the electronic structures are not clear yet.

With these experimental results in mind, in this paper we show first the electronic band structure of $(PbSe)_5(Bi_2Se_3)_6$ by first-principles calculations. We find that this material has topological interface states in the bulk, presenting a gapped Dirac-like energy dispersion of Bi_2Se_3 layers capped by PbSe layers. Second, we show from defect energy analyses that a high density of Bi_{Pb} antisite defects can actually be included in real materials. We find strong influences of Bi_{Pb} antisite defects on the electronic band structure near the Fermi energy, showing that Bi_{Pb} modifies energy band alignments between Bi_2Se_3 and PbSe states. This inference points to an interesting possibility for band-structure tuning in topological-material heterostructures via defect chemistry.

II. METHODS

Figure 1(a) shows the crystal structure of $(PbSe)_5(Bi_2Se_3)_6$. In this paper, we choose the lattice axes setting of $A2/m$ with the experimental lattice constants of $(a,b,c) = (21.551,52.918,4.1774)$ Å and $\gamma = 107.224^\circ$ [4]. The atomic coordinates have been experimentally reported only for $(Ag_{0.2}Pb_{0.8}Se)_5(Bi_2Se_3)_6$ [4]. Using the experimental atomic coordinates by substituting Ag with Pb, we prepare an initial structure of $(PbSe)_5(Bi_2Se_3)_6$. The atomic positions are fully optimized until forces acting on every atom become smaller than 10 mRy/Bohr by the first-principles calculations, given that the band-structure changes due to atomic relaxations are small enough. The conventional unit cell contains 160 atoms/cell. As discussed later, it is essential to take account of the impacts of Bi_{Pb} defects on the electronic structures, which are also calculated using the same unit-cell size.

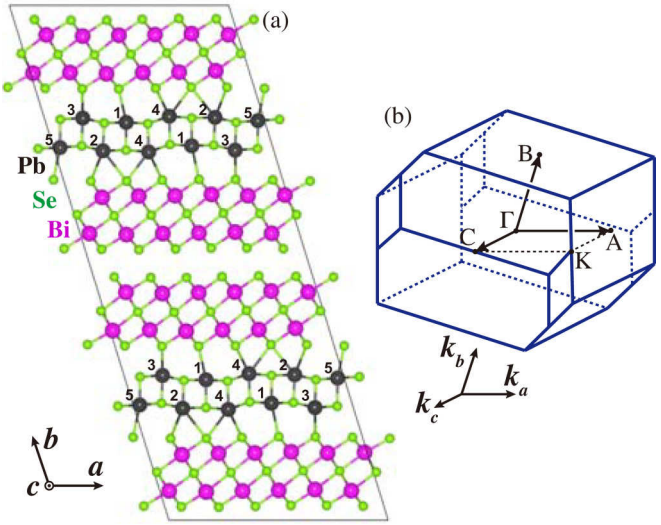

FIG. 1. (a) Crystal structure of $(PbSe)_5(Bi_2Se_3)_6$ and (b) its Brillouin zone with the **k** labels defined in this study. In the crystal structure, small (green), medium (gray), and large (purple) spheres show Se, Pb, and Bi atoms, respectively, and the symmetrically equivalent Pb-site labels are shown.

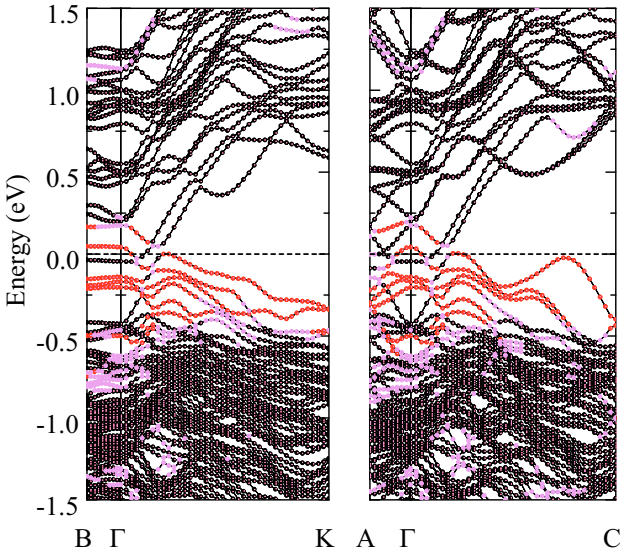

FIG. 2. Layer-resolved band structure of $(PbSe)_5(Bi_2Se_3)_6$. The energy origin is taken at the Fermi level. The wave-function characters spatially dominated by Bi_2Se_3 (black), PbSe (red), and both layers (magenta) are shown in the respective color.

The first-principles calculations are based on the density-functional theory (DFT) within the local-density approximation (LDA) [15]. The Kohn-Sham equations are self-consistently solved using the all-electron full-potential linearized augmented-plane-wave (FLAPW) method, and the spin-orbit coupling (SOC) is included self-consistently as a second variation method [16–22]. Computations are done using the HiLAPW code, which utilizes the Soler-Williams-type LAPW basis functions [23,24]. We use the cutoff energies of 10 and 40 Ry for the wave function and potential basis sets, respectively, and the **k** mesh of $1 \times 1 \times 4$. We set the muffin-tin radius of 1.0 Å for all elements, and we use the spherical-wave cutoff of the Soler-Williams basis in muffin-tin spheres of $l_{\max}^{\mathrm{SW}} = 2$ for wave functions, and the spherical part for electron densities, respectively. To check the computational accuracy, we also perform the first-principles FLAPW calculations of $(PbSe)_5(Bi_2Se_3)_6$ using the FLEUR code [25]. In the FLEUR calculations, we use the cutoff parameters of angular momentum $l_{\max} = 10$, wave-function basis $K_{\max} = 3.2$ Bohr^{-1}, and muffin-tin radii 2.67 Bohr for Bi and 2.51 Bohr for Pb and Se. This crosscheck allowed us to confirm that both codes give basically the same conclusions for $(PbSe)_5(Bi_2Se_3)_6$ [26].

We calculate the topological invariants from the first principles for bulk Bi_2Se_3 ($R\bar{3}m$) and PbSe ($Fm\bar{3}m$) with the experimental structures using the parity eigenvalues at the time-reversal invariant momenta [27]. We confirm that the calculated topological invariants $(\nu; \nu_1\nu_2\nu_3)$ are (1;000) for Bi_2Se_3 and (0;000) for PbSe, showing a strong topological and an ordinary insulator, respectively.

III. RESULTS AND DISCUSSION

A. $(PbSe)_5(Bi_2Se_3)_6$

Figure 2 shows the calculated band structure of $(PbSe)_5(Bi_2Se_3)_6$ along the **k** path defined in Fig. 1(b). To clarify the atomistic characters of bands, we plot the layer-resolved band in the figure, which shows the dominant wave-function contributions from Bi_2Se_3, PbSe, and both layers to each eigenstate.

The band structure of $(PbSe)_5(Bi_2Se_3)_6$ shows a metallic feature with four degenerated bands crossing the Fermi energy around the Γ point. The layer-resolved band shows a mixture of the Bi_2Se_3- and PbSe-layer bands near the Fermi energy region. The PbSe-layer bands lie dominantly just below the Fermi energy, and two of them are partially filled with holes around Γ. In the conduction-band region higher than about 0.7 eV, there are some parabolic bands of PbSe layers, indicative of the 0.7 eV band gap of the PbSe layers (see below). Two dispersing bands that originated from Bi_2Se_3 layers also cross the Fermi energy, and one of them appears to be a Dirac-cone-like energy dispersion along the in-plane **k** path (on the k_a–k_c plane) with the Dirac-like point at −0.41 eV at Γ. This Dirac-like dispersion is quite similar in nature to those calculated for free-standing Bi_2Se_3 slabs [28,29], as discussed in the next paragraph. Note that the bottom of the Dirac-cone dispersion does not exactly touch the concave part of the M-shaped band at Γ, and there is a tiny gap of 0.02 eV [26]. This is probably because of the hybridization between the states in the upper and lower interfaces, considering that the hybridization gap is induced at the Dirac point for a free-standing Bi_2Se_3 slab with 2QL thickness [28]. The calculated hybridization gap of 0.02 eV in $(PbSe)_5(Bi_2Se_3)_6$ is smaller than that of the Bi_2Se_3 2QL slab at the equilibrium structure (typically 0.1–0.2 eV [28]) by an order of magnitude. This is because the Bi_2Se_3 layers in $(PbSe)_5(Bi_2Se_3)_6$ are strained by a lattice mismatch with the PbSe layers, and expanded in the in-plane direction by a few percent relative to the bulk Bi_2Se_3 lattice. The previous calculations for the Bi_2Se_3 slabs have shown that the hybridization gap at the Dirac point at Γ becomes smaller (and the M-shape feature of the valence band

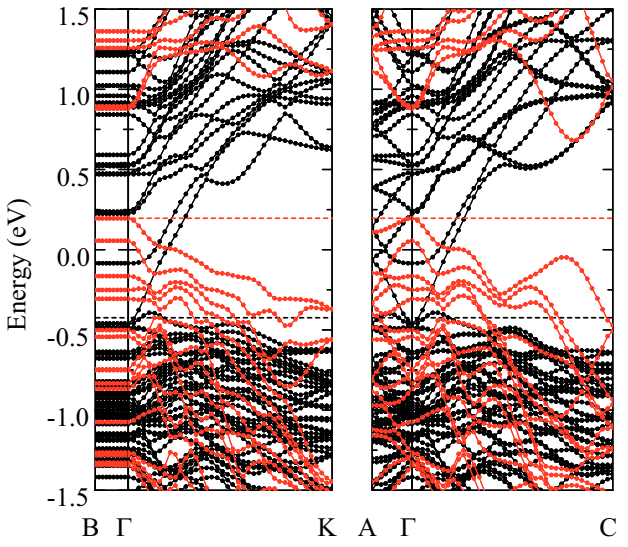

FIG. 3. Band structures of the two 2QL-$(Bi_2Se_3)_6$ slab (black solid circles) and the two bilayer-$(PbSe)_5$ slab (red solid circles). The Fermi energy for the Bi_2Se_3 slab at -0.42 eV and the valence-band top energy for the PbSe slab at $+0.20$ eV are shown by dashed lines, and the relative energy position is adjusted so as to match with Fig. 2.

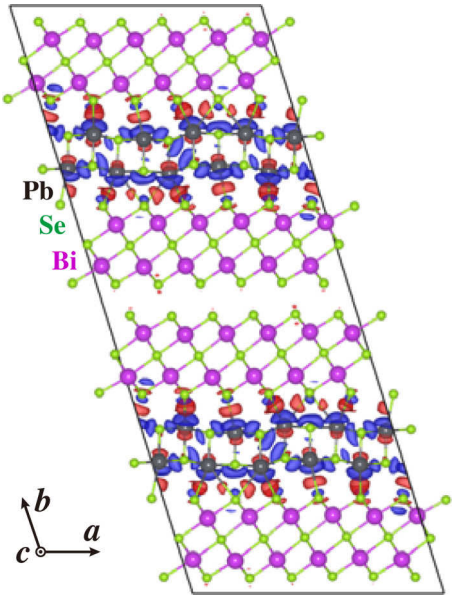

FIG. 4. Charge-density difference between $(PbSe)_5(Bi_2Se_3)_6$ and the superposition of the building-block slabs used for Fig. 3. Isosurface densities of $\pm 0.65 \times 10^{-3}$ electrons/Bohr ^{3} are plotted, and the positive (red) and negative (blue) values show that the electron density increases and decreases in $(PbSe)_5(Bi_2Se_3)_6$, respectively.

becomes more pronounced) as the in-plane lattice constant increases from the equilibrium value [30]. The calculated bands in the $B-\Gamma$ direction are almost flat, showing a roughly flat two-dimensional nature of the bulk electronic structure of this material.

To more clearly compare the band characters of $(PbSe)_5(Bi_2Se_3)_6$ with those of the building block layers, we calculate the band structures of isolated 2QL-Bi_2Se_3 and bilayer-PbSe slabs. We use slab models with the same lattice as $(PbSe)_5(Bi_2Se_3)_6$, from which all PbSe or Bi_2Se_3 layers are simply removed for modeling the isolated 2QL-Bi_2Se_3 and bilayer-PbSe, respectively. The model consists of two 2QL-$(Bi_2Se_3)_6$ slabs or two bilayer-$(PbSe)_5$ slabs in the cell, and we keep atoms in the same positions. Figure 3 shows the calculated band structures of the bilayer-$(PbSe)_5$ and 2QL-$(Bi_2Se_3)_6$ slabs, where the relative energy between two systems is shifted by $+0.20$ and -0.42 eV from each Fermi energy, respectively. As a consequence of such a band energy shift, the superimposed band structures shown in Fig. 3 well represent the $(PbSe)_5(Bi_2Se_3)_6$ band of Fig. 2. Considering the relative energy shifts necessary for this agreement, we can speculate that electrons are slightly donated from PbSe to Bi_2Se_3 layers in $(PbSe)_5(Bi_2Se_3)_6$ by about 0.6 electron/cell relative to the isolated building blocks.

Comparing the band structures shown in Figs. 2 and 3, we can find that the electronic states of $(PbSe)_5(Bi_2Se_3)_6$ basically keep the two-dimensional slab character of the respective building block layers. The band structure of the PbSe slab shows an insulating nature with the gap at Γ of 0.68 eV, as expected from the fact that PbSe is an ordinary insulator. PbSe monolayers (or stacks of them) are topological crystalline insulators [31], but the bilayer in $(PbSe)_5(Bi_2Se_3)_6$ is probably trivial. Bi_2Se_3 is a topological insulator, and the Bi_2Se_3 slab has topological Dirac-cone surface states with the Dirac-like point close to the Fermi energy. Such an insulating gap of the PbSe slab and the topological state of the Bi_2Se_3 slab are retained even in the heterostructure $(PbSe)_5(Bi_2Se_3)_6$ as found in Fig. 2. Therefore, we theoretically conclude that $(PbSe)_5(Bi_2Se_3)_6$ actually has the topological Dirac-cone interface states originating from the Bi_2Se_3 layers encapsulated by the PbSe block layers in the bulk.

Recently, Bi_1Te_1, which consists of an alternating layered structure of Bi_2Te_3 and Bi, has been found to be a dual three-dimensional topological insulator where a weak topological insulator and topological crystalline insulator phases appear simultaneously [32]. In Bi_1Te_1, the band inversion between Bi_2Te_3- and Bi-layer states around the Fermi level is the key mechanism of emergence of the topological character. In the band structure of $(PbSe)_5(Bi_2Se_3)_6$ shown in Fig. 2, we find that two PbSe and Bi_2Se_3 bands are inverted around the Fermi level at Γ, and the parity exchanges take place twice at Γ. This result may suggest the nontopological characters of $(PbSe)_5(Bi_2Se_3)_6$, although the topological indices cannot be exactly calculated because of the metallic features of bands.

To estimate the size of the interaction between the building block layers, we calculate the interface energy per unit area as $E_{\rm int} = (E_{\rm bulk} - E_{\rm slab})/(4ac)$, where $E_{\rm bulk}$ is the total energy of the bulk $(PbSe)_5(Bi_2Se_3)_6$, and $E_{\rm slab}$ is the total energy sum of the $(PbSe)_5$ and $(Bi_2Se_3)_6$ slabs. The denominator $(4ac)$ stands for $E_{\rm int}$ per unit area in one interface because the conventional cell includes four PbSe-Bi_2Se_3 interfaces. The calculated $E_{\rm int}$ of $-6\,{\rm meV}/{\rm \AA}^2$ shows a small energy gain of the bulk $(PbSe)_5(Bi_2Se_3)_6$ heterostructure, showing weak interaction between the building block layers.

Figure 4 shows the charge-density difference between $(PbSe)_5(Bi_2Se_3)_6$ and the superposition of the isolated building block slabs. The result shows that, by forming the heterostructure, the electrons of mainly Pb atoms in the PbSe

layers transfer to the interstitial regions between the PbSe and Bi_2Se_3 layers. The transferred electrons are located mainly between Pb atoms of PbSe and Se atoms of Bi_2Se_3 connecting the interfaces, indicating that electronic bonds are formed between the building block layers. Considering that $(PbSe)_5(Bi_2Se_3)_6$ is slightly stable in energy relative to the separated building block layers, the electronic bonding makes the heterostructure stable, overcoming competition with an energy loss due to the hole injections into the PbSe valence bands. However, the estimated number of transferred electrons is very small, contributing to a very small energy gain in the heterostructure.

ARPES experiments have shown that topological interface states exist in $(PbSe)_5(Bi_2Se_3)_6$ [2,3]. One major difference between our calculation and the ARPES experiment is that the PbSe bands near the Fermi energy shown in Fig. 2 have not been observed in the experiment. A possible reason for the difference is that ARPES observes surface regions of cleaved samples, and it has been expected that the topmost layer of the cleaved surface is a Bi_2Se_3 QL [2,3], thus being sensitive to the Bi_2Se_3 states. Though surface calculations are necessary for a detailed comparison with the ARPES bands, our calculation of the bulk $(PbSe)_5(Bi_2Se_3)_6$ shows the Dirac-cone dispersion of Bi_2Se_3 layers, and the Bi_2Se_3-layer bands look quite similar to those observed by ARPES.

Another possibility for the origin of the discrepancy between our calculation and the ARPES result can be inferred from the fact that a recent experiment has shown that a high density of Bi_{Pb} antisite defects exists in real $(PbSe)_5(Bi_2Se_3)_6$ samples [6], as mentioned in the Introduction. Bi_{Pb} can change the electronic structure such as a band alignment between the Bi_2Se_3 and PbSe layers. Because Bi_{Pb} can act as electron donors and the nominal ionic valence Bi^{3+} is higher than Pb^{2+}, one can speculate that the PbSe bands may shift lower in energy relative to the Bi_2Se_3 bands. Thus, the PbSe bands may be gone from the region near the Fermi energy in $(PbSe)_5(Bi_2Se_3)_6$ with Bi_{Pb} defects. To confirm the above scenario, we discuss the effects of Bi_{Pb} on the electronic structure in the next subsection.

On the structural stability of $(PbSe)_5(Bi_2Se_3)_6$, we have calculated the formation energies, assuming the reactions as

$$\begin{aligned} &5\mathrm{Pb(g)} + 12\mathrm{Bi(g)} + 23\mathrm{Se(g)} \\ &\rightarrow 5\mathrm{Pb(s)} + 12\mathrm{Bi(s)} + 23\mathrm{Se(s)} \\ &\rightarrow 5\mathrm{PbSe} + 6\mathrm{Bi_2Se_3} \\ &\rightarrow (\mathrm{PbSe})_5(\mathrm{Bi_2Se_3})_6, \end{aligned} \quad (1)$$

where the reactions proceed from gas phases (g) via elementary solid phases (s) and binary solid phases to $(PbSe)_5(Bi_2Se_3)_6$. We calculate the formation energies using the DFT total energy difference between before and after each reaction, where the neutral isolated atoms and the elementary solid in their stable form are used for gas and elementary solid phases, respectively. The calculated formation energies of each reaction step are -3.28, -0.26, and -0.02 eV/atom [26], showing that $(PbSe)_5(Bi_2Se_3)_6$ is most stable relative to the other mixed phases.

B. $(Bi_xPb_{1-x}Se)_5(Bi_2Se_3)_6$

To clarify the influence of defects on the electronic structure, we calculate the band structures of $(Bi_xPb_{1-x}Se)_5(Bi_2Se_3)_6$ models, which include Bi_{Pb} antisite defects in the PbSe layers.

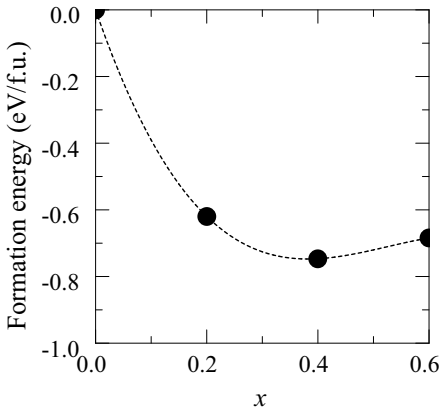

FIG. 5. Defect formation energy of Bi_{Pb} antisite defects in the $(Bi_xPb_{1-x}Se)_5(Bi_2Se_3)_6$ models.

We use the same unit-cell size as $(PbSe)_5(Bi_2Se_3)_6$, but some of the Pb sites are replaced with Bi keeping the crystal symmetry of $(PbSe)_5(Bi_2Se_3)_6$. In our models, Bi_{Pb} defects occupy the Pb(1) site for $x = 0.2$, the Pb(1, 5) sites for $x = 0.4$, and the Pb(1, 2, 5) sites for $x = 0.6$ [see the Pb-site labels in Fig. 1(a)], respectively. The atomic positions are fully optimized with the fixed lattice constants and the same optimization criterion as in the calculations without defects. For $x = 0.2$, we also adopt another model with the Pb(2)-site filled with Bi, revealing a higher total energy by 0.23 eV/f.u. but a similar band structure as compared to the original model.

To clarify the energy stability of Bi_{Pb} defects, we calculate the defect formation energy (E_x) as

$$\begin{aligned} E_x = {} & E[(\mathrm{Bi}_x\mathrm{Pb}_{1-x}\mathrm{Se})_5(\mathrm{Bi_2Se_3})_6] \\ & - E[(\mathrm{PbSe})_5(\mathrm{Bi_2Se_3})_6] - 5xE[\mathrm{Bi}] + 5xE[\mathrm{Pb}], \end{aligned} \quad (2)$$

where $E[X]$ is the total energy of a material X per formula unit, and the reference total energies are calculated for bulk Bi (space group $R\bar{3}m$) and Pb ($Fm\bar{3}m$) in their stable phases with the experimental structures. Figure 5 shows the calculated E_x as a function of x. As E_x shows negative values, Bi_{Pb} can be intrinsically included in the system. We estimate a theoretically optimized Bi_{Pb} concentration giving the energy minimum at $x = 0.38$ from the polynomial fitting curve, consistent with the experimentally observed value of $x = 0.31$ in the samples [6].

Figure 6 shows the calculated band structure of the $(Bi_xPb_{1-x}Se)_5(Bi_2Se_3)_6$ models for $x = 0$, 0.2, and 0.4. Zooms of the band structure near the Fermi energy are plotted in Fig. 7. We find a strong effect of Bi_{Pb} on the energy alignment between Bi_2Se_3 and PbSe (i.e., $Bi_xPb_{1-x}Se$) -layer bands. The overall shapes of the Bi_2Se_3-layer bands are basically rigid in nature, and slightly shift lower in energy with increasing x. All models have the topological Dirac-cone interface state, and the energy of the pseudo-Dirac point at Γ ($E^{\mathrm{DP}(\Gamma)}_{\mathrm{Bi_2Se_3}}$) gradually shifts from -0.41 eV for $x = 0$ to -0.65 eV for $x = 0.4$ as plotted in Fig. 6(d). The PbSe-layer bands show a much larger downward shift in energy, and the PbSe valence bands for $x = 0$ near the Fermi energy are buried into the Bi_2Se_3 valence bands below $E^{\mathrm{DP}(\Gamma)}_{\mathrm{Bi_2Se_3}}$ for $x = 0.4$. In Fig. 6(d), we plot the corresponding valence-band top and conduction-band bottom

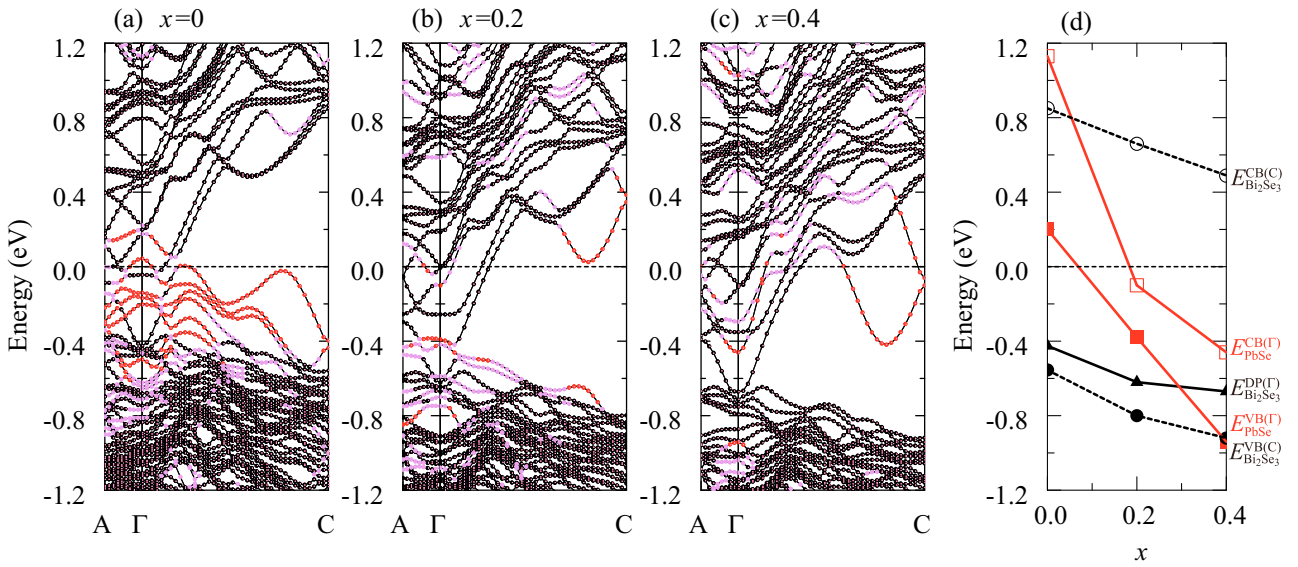

FIG. 6. Layer-resolved band structures of the $(Bi_xPb_{1-x}Se)_5(Bi_2Se_3)_6$ models for (a) $x = 0$, (b) $x = 0.2$, and (c) $x = 0.4$. The wave-function characters spatially dominated by Bi_2Se_3 (black), $Bi_xPb_{1-x}Se$ (red), and both layers (magenta) are shown in their respective color. The Fermi energy is set to be the energy zero. (d) The energy levels at Γ of the Bi_2Se_3 Dirac-like points $E^{DP(\Gamma)}_{Bi_2Se_3}$ (black triangles), the PbSe valence-band top $E^{VB(\Gamma)}_{PbSe}$ (red solid squares), and the PbSe conduction-band bottom $E^{CB(\Gamma)}_{PbSe}$ (red open squares). The energy levels at C of the Bi_2Se_3 highest occupied state $E^{VB(C)}_{Bi_2Se_3}$ (black solid circles) and the lowest unoccupied state $E^{CB(C)}_{Bi_2Se_3}$ (black open circles) are also shown.

energies at Γ ($E^{VB(\Gamma)}_{PbSe}$ and $E^{CB(\Gamma)}_{PbSe}$) of the $Bi_xPb_{1-x}Se$-layer bands, showing the strong energy shift upon introducing the Bi_{Pb} defects. Instead, the PbSe conduction bands appear near the Fermi energy, resulting in one and two bands being partially occupied for $x = 0.2$ and 0.4, respectively. As a consequence of the strongly shifted PbSe-layer bands, the band structure near the Fermi energy region becomes clearer in the system with Bi_{Pb}, compared with that of $x = 0$. This result shows that the element substitutions in $(PbSe)_5(Bi_2Se_3)_6$ can significantly modify the electronic structure near the Fermi energy. The Bi_{Pb} defects do not drastically change the Bi_2Se_3 bands near the Fermi energy at Γ. To show the effect of Bi_{Pb} on the Bi_2Se_3 bands, we plot the valence-band top and conduction-band bottom energies of the Bi_2Se_3-layer bands at the zone boundary point C ($E^{VB(C)}_{Bi_2Se_3}$ and $E^{CB(C)}_{Bi_2Se_3}$) in Fig. 6(d), which demonstrates that $E^{VB(C)}_{Bi_2Se_3}$ and $E^{CB(C)}_{Bi_2Se_3}$ get lower in energy with increasing x. The energy position of $E^{DP(\Gamma)}_{Bi_2Se_3}$ slightly shifts upward relative to $E^{VB(C)}_{Bi_2Se_3}$.

Recently, the topological-insulator-based superconductor $Cu_x(PbSe)_5(Bi_2Se_3)_6$, in which Cu atoms are placed in the van der Waals gap regions between the Bi_2Se_3 layers, has

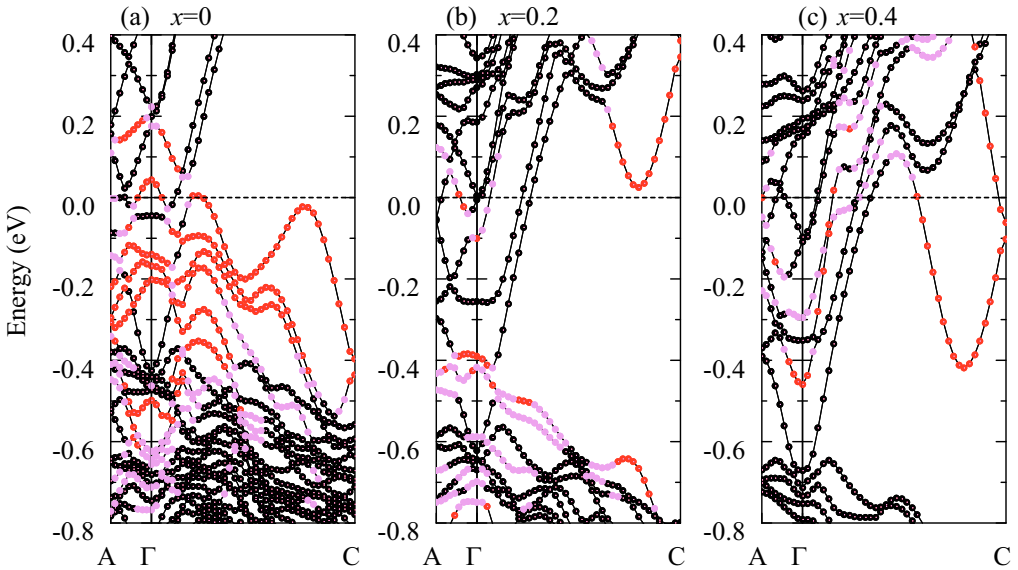

FIG. 7. Layer-resolved band structures magnified near the Fermi energy of the $(Bi_xPb_{1-x}Se)_5(Bi_2Se_3)_6$ models for (a) $x = 0$, (b) $x = 0.2$, and (c) $x = 0.4$. The color coding of the bands corresponds to Fig. 6. Note that band symmetries are not considered for the line connections.

been studied experimentally [14]. Our calculations for the $(PbSe)_5(Bi_2Se_3)_6$ systems show that the topological Bi_2Se_3 states are well protected by the nontopological PbSe units in the heterostructure, supporting the primary expectation that $Cu_x(PbSe)_5(Bi_2Se_3)_6$ shows a similar nature to that of $Cu_xBi_2Se_3$ [14].

IV. SUMMARY

In summary, we have studied the electronic band structures of the natural heterostructure $(PbSe)_5(Bi_2Se_3)_6$ with and without Bi_{Pb} antisite defects. The electronic structure of $(PbSe)_5(Bi_2Se_3)_6$ near the Fermi energy consists of a mixture of Bi_2Se_3- and PbSe-layer bands, and we find that the Dirac-cone-type energy dispersion originates from Bi_2Se_3 layers capped by PbSe block layers. Defect formation energy analysis shows that a high density of Bi_{Pb} antisite defects can be included in real materials, with the optimum composition $(Bi_xPb_{1-x}Se)_5(Bi_2Se_3)_6$ with $x \sim 0.38$. Even if the defects exist in the material, the topological interface states are kept as the Dirac-cone-like dispersion in the electronic structure of $(Bi_xPb_{1-x}Se)_5(Bi_2Se_3)_6$ near the Fermi energy. The Bi_{Pb} antisite defects have a strong effect on the band structure, and the PbSe bands shift down more strongly in energy than the Bi_2Se_3 bands with increasing x. This exposes the topological surface state at 0.5 eV below the Fermi level that is overlapping with the PbSe derived bands in the stoichiometric compound.

ACKNOWLEDGMENTS

We would like to thank Gregor Michalicek and Christian-Roman Gerhorst for the technical support of FLEUR calculations. This work was supported by JSPS ("Program for Advancing Strategic International Networks to Accelerate the Circulation of Talented Researchers", and KAKENHI Grants No. JP15H05853, No. JP16H02267, and No. JP17H06154), MEXT (the Research Program of "Five-star Alliance" in "NJRC Mater. & Dev."), and DFG (CRC1238 "Control and Dynamics of Quantum Materials," Projects A04 and C01). The computation in this work was partly done using the facilities of the Supercomputer Center, the Institute for Solid State Physics, the University of Tokyo. H.M. gratefully acknowledges the hospitality of Forschungszentrum Jülich, where part of this work was completed.

[1] Y. Ando, J. Phys. Soc. Jpn. **82**, 102001 (2013).
[2] K. Nakayama, K. Eto, Y. Tanaka, T. Sato, S. Souma, T. Takahashi, K. Segawa, and Y. Ando, Phys. Rev. Lett. **109**, 236804 (2012).
[3] K. Nakayama, H. Kimizuka, Y. Tanaka, T. Sato, S. Souma, T. Takahashi, S. Sasaki, K. Segawa, and Y. Ando, Phys. Rev. B **92**, 100508(R) (2015).
[4] L. Fang, C. C. Stoumpos, Y. Jia, A. Glatz, D. Y. Chung, H. Claus, U. Welp, W.-K. Kwok, and M. G. Kanatzidis, Phys. Rev. B **90**, 020504(R) (2014).
[5] S. Sasaki, K. Segawa, and Y. Ando, Phys. Rev. B **90**, 220504(R) (2014).
[6] K. Segawa, A. A. Taskin, and Y. Ando, J. Solid State Chem. **221**, 196 (2015).
[7] M. G. Kanatzidis, Acc. Chem. Res. **38**, 367 (2005).
[8] Y. Zhang, A. P. Wilkinson, P. L. Lee, S. D. Shastri, D. Shu, D.-Y. Chung, and M. G. Kanatzidis, J. Appl. Cryst. **38**, 433 (2005).
[9] H. Zhang, C.-X. Liu, X.-L. Qi, X. Dai, Z. Fang, and S.-C. Zhang, Nat. Phys. **5**, 438 (2009).
[10] I. Aguilera, C. Friedrich, G. Bihlmayer, and S. Blügel, Phys. Rev. B **88**, 045206 (2013).
[11] I. A. Nechaev, R. C. Hatch, M. Bianchi, D. Guan, C. Friedrich, I. Aguilera, J. L. Mi, B. B. Iversen, S. Blügel, Ph. Hofmann, and E. V. Chulkov, Phys. Rev. B **87**, 121111(R) (2013).
[12] P. Dziawa, B. J. Kowalski, K. Dybko, R. Buczko, A. Szczerbakow, M. Szot, E. Łusakowska, T. Balasubramanian, B. M. Wojek, M. H. Berntsen, O. Tjernberg, and T. Story, Nat. Mater. **11**, 1023 (2012).
[13] A. A. Burkov and L. Balents, Phys. Rev. Lett. **107**, 127205 (2011).
[14] M. Sato and Y. Ando, Rep. Prog. Phys. **80**, 076501 (2017).
[15] J. F. Janak, V. L. Moruzzi, and A. R. Williams, Phys. Rev. B **12**, 1257 (1975).
[16] D. D. Koelling and G. O. Arbman, J. Phys. F **5**, 2041 (1975).
[17] O. K. Andersen, Phys. Rev. B **12**, 3060 (1975).
[18] D. D. Koelling and B. N. Harmon, J. Phys. C **10**, 3107 (1977).
[19] A. H. MacDonald, W. E. Pickett, and D. D. Koelling, J. Phys. C **13**, 2675 (1980).
[20] M. Weinert, J. Math. Phys. **22**, 2433 (1981).
[21] E. Wimmer, H. Krakauer, M. Weinert, and A. J. Freeman, Phys. Rev. B **24**, 864 (1981).
[22] M. Weinert, E. Wimmer, and A. J. Freeman, Phys. Rev. B **26**, 4571 (1982).
[23] J. M. Soler and A. R. Williams, Phys. Rev. B **40**, 1560 (1989).
[24] J. M. Soler and A. R. Williams, Phys. Rev. B **42**, 9728 (1990).
[25] http://www.flapw.de.
[26] The FLEUR calculation of $(PbSe)_5(Bi_2Se_3)_6$ gives a hybridization gap of 0.07 eV at the Dirac-like point of the Bi_2Se_3 layer at Γ. The formation energies of each reaction step in Eq. (1) are calculated to be −3.57, −0.46, and −0.002 eV/atom by FLEUR.
[27] L. Fu and C. L. Kane, Phys. Rev. B **76**, 045302 (2007).
[28] O. V. Yazyev, J. E. Moore, and S. G. Louie, Phys. Rev. Lett. **105**, 266806 (2010).
[29] H. Jin, J.-H. Song, and A. J. Freeman, Phys. Rev. B **83**, 125319 (2011).
[30] H. Aramberri and M. C. Muñoz, Phys. Rev. B **95**, 205422 (2017).
[31] Y. Kim, C. L. Kane, E. J. Mele, and A. M. Rappe, Phys. Rev. Lett. **115**, 086802 (2015).
[32] M. Eschbach, M. Lanius, C. Niu, E. Młyńczak, P. Gospodarič, J. Kellner, P. Schüffelgen, M. Gehlmann, S. Döring, E. Neumann, M. Luysberg, G. Mussler, L. Plucinski, M. Morgenstern, D. Grützmacher, G. Bihlmayer, S. Blügel, and C. M. Schneider, Nat. Commun. **8**, 14976 (2017).